Springer

KSME

Journal of Mechanical Science and Technology 26 (1) (2012) 283~297
www.springerlink.com/content/1738-494x
DOI 10.1007/s12206-011-1037-0

Turbulence modeling of natural convection in enclosures: A review †

Seok-Ki Choi* and Seong-O Kim

Korea Atomic Energy Research Institute, Fast Reactor Development Division, 150-1 Deokjin-dong, Yuseong-gu, Daejeon, 305-353, Korea

(Manuscript Received April 22, 2011; Revised October 16, 2011; Accepted November 19, 2011)

Abstract

In this paper a review of recent developments of turbulence models for natural convection in enclosures is presented. The emphasis is placed on the effect of the treatments of Reynolds stress and turbulent heat flux on the stability and accuracy of the solution for natural convection in enclosures. The turbulence models considered in the preset study are the two-layer $k-\varepsilon$ model, the shear stress transport (SST) model, the elliptic-relaxation (V2-f) model and the elliptic-blending second-moment closure (EBM). Three different treatments of the turbulent heat flux are the generalized gradient diffusion hypothesis (GGDH), the algebraic flux model (AFM) and the differential flux model (DFM). The mathematical formulation of the above turbulence models and their solution method are presented. Evaluation of turbulence models are performed for turbulent natural convection in a 1:5 rectangular cavity ($Ra = 4.3\times10^{10}$) and in a square cavity with conducting top and bottom walls ($Ra = 1.58\times10^{9}$) and the Rayleigh-Benard convection ($Ra = 2\times10^{6} \sim Ra = 10^{9}$). The relative performances of turbulence models are examined and their successes and shortcomings are addressed.

Keywords: Turbulence models; Natural convection flows; Thermal stratification; Rayleigh-Benard convection

1. Introduction

Accurate prediction of natural convection flows is very important for investigating various engineering applications such as cooling of electronic packages, solar collector, building ventilation and passive heat removal system of a liquid metal nuclear reactor. For natural convection flows there are little experimental data to validate turbulence models, mainly due to experimental difficulties. It is still difficult to measure the turbulent heat fluxes and the low velocities accurately and to achieve the ideal adiabatic condition. The Rayleigh number of most practical flows for engineering applications is at least larger than $Ra \approx 10^{10}$ and the DNS (direct numerical simulation) or LES (large eddy simulation) methods can not applied to these practical engineering flows. Most works in the literature employ the RANS (Reynolds averaged Navier-Stokes) equation approach. In the RANS equation approach, the choice of turbulence model is crucial, as it directly affects the accuracy of the solutions. However, the turbulence modeling of natural convection flows is still difficult and the rationale for the difficulties is well explained in Hanjalic [1].

Earlier computations of natural convection were done by the standard $k-\varepsilon$ model with wall function method. The difficulty of computing the turbulent natural convection by the conventional $k-\varepsilon$ model with the wall function method is the validity of the wall functions, which are based on the local equilibrium logarithmic velocity and temperature assumptions. The logarithmic wall functions were originally derived for the forced-convection flows and do not hold for the natural flows. The other difficulty is that the standard $k-\varepsilon$ model predicts excessive turbulence eddy viscosity near the wall as evidenced by Heindel et al. [2]. Due to these problems, many previous authors used the low-Reynolds-number turbulence models for computation of natural convection flows.

There exist several turbulence models in the literature which calculate all the way to the wall without using the wall function method. Due to the limited space allowed in this paper only a few turbulence models widely used at present will be briefly mentioned here. The several low-Reynolds number turbulence models are developed by many authors and one of these models widely used at present is the Launder and Sharma model [3]. However, the low-Reynolds number models contain the ad-hoc damping functions in the definition of eddy viscosity and in the equation of the turbulence kinetic energy dissipation rate, and it is well known that the models do not work well in the adverse pressure gradient region. The other way to avoid the deficiency of the wall function method is to use the one-equation model near the wall instead of the wall functions. Such a two-layer model was developed by Chen and Patel [4]. Medic and Durbin [5] developed an elliptic relaxation (V2-f) model in which two more partial differential equations are solved to determine the velocity

† This paper was recommended for publication in revised form by Associate Editor Jun Sang Park

* Corresponding author. Tel.: +82 42 868 2993, Fax.: +82 42 861 7697
E-mail address: skchoi@kaeri.re.kr

scale in the expression of turbulence eddy viscosity. Choi et al. [6] applied this model to the computation of natural convection in a rectangular cavity and showed that this model outperforms the conventional $k-\varepsilon$ models. The other turbulence model currently used by many authors is the shear stress transport (SST) model by Menter [7]. The SST model is a blending model between the $k-\varepsilon$ model and the $k-\omega$ model such that the model behaves as the $k-\omega$ model in the near wall region and as the $k-\varepsilon$ model in the outer region. Thus, this model cured the deficiency of the $k-\omega$ model in the computation of the outer region. Application of the SST model to the computation of natural convection flows is rarely seen in the literature and is given in the present study.

It is noted that the implementation of the wall reflection terms in the general purpose code that can handle the complex geometries is very difficult. This difficulty is due to the existence of wall-related parameters such as the wall normal vector and the wall shear stress at the nearest wall from the calculation point, and the difficulty is not due to the solution method for the transport equations for the Reynolds stresses or turbulent heat fluxes. The second-moment closure free from the wall related parameters is the elliptic-blending model (EBM) by Thielen et al. [8]. Recently Choi and Kim [9] obtained numerical solutions for a natural convection in a 1:5 rectangular cavity experimented by King [10] using this model, and showed that the solution by the EBM is superior to those by the two-equation models. It is also noted that the V2-f model by Durbin [5] is free from the wall-related parameters.

The other difficulty in predicting the turbulent natural convection is the treatment of the turbulent heat fluxes. If one does not use the differential heat flux model, a proper way of treating the turbulent heat fluxes should be sought. In the earlier stage of works the authors used a simple gradient diffusion hypothesis (SGDH) in treating the turbulent heat fluxes. However, it does not work well for natural convection flows. Thus, Ince and Launder [11] proposed a generalized gradient diffusion hypothesis (GGDH) to overcome this deficiency of the SGDH assumption. As will be shown later, the GGDH works very well for shear dominant flows, however, it produces unstable and inaccurate solutions for strongly stratified natural convection flows. To remedy this deficiency, Kenjeres and Hanjalic [12] developed an algebraic flux model (AFM). The main difference between the AFM and the GGDH is the inclusion of the temperature variance term in the algebraic expression of the turbulent heat fluxes. This inclusion of temperature variance term stabilizes the overall solution process and results in stable and accurate solutions. It may be commonly accepted that the use of the second-moment closure may result in better solutions for natural convection flows. The second-moment modeling of a natural convection requires the modeling of various terms in the transport equations for the turbulent heat flux vector, the temperature variance and the dissipation rate of the temperature variance. Since the second-moment closure computes the Reynolds stresses more accurately than the two-equation turbulence models, and it usually produces better solutions. The low-Reynolds number second-moment closures applied to the analysis of the turbulent natural convection are rarely seen in the literatures and the examples using the near wall second-moment closure are the works by Peeters and Henkes [13], Dol and Hanjalic [14] and Choi et al. [15]. Shin et al. [16] also developed a differential flux model (DFM) based on the elliptic-blending model by Thielen et al. [8] where the differential equations are solved for the turbulent heat fluxes. It is noted that the second-moment closure used by Dol and Hanjalic [14] or Choi et al. [15] is different from the DFM by Shin et al. [16] in that the latter model does not include any wall-related parameters.

The objective of the present paper is to review current advances of turbulence models for natural convection flows. A brief introduction is given above, and the mathematical formulation of turbulence models together with their validation will be given in the following sections.

2. Governing equations

The ensemble-averaged governing equations for a conservation of the mass, momentum and energy can be written as follows:

$$\frac{D}{Dt}(\rho)=0 \tag{1}$$

$$\frac{D}{Dt}(\rho U_i)=-\frac{\partial p}{\partial x_i}+\frac{\partial}{\partial x_j}\left(\mu\frac{\partial U_i}{\partial x_j}-\rho\overline{u_iu_j}\right)-\rho\beta g_i(\Theta-\Theta_{ref}) \tag{2}$$

$$\frac{D}{Dt}(\rho\Theta)=\frac{\partial}{\partial x_j}\left(\frac{\mu}{\mathrm{Pr}}\frac{\partial\Theta}{\partial x_j}-\rho\overline{\theta u_j}\right) \tag{3}$$

where $\overline{u_iu_j}$ are the Reynolds stresses and $\overline{\theta u_j}$ are the turbulent heat fluxes which should be modeled. Different turbulence model means different treatment of the Reynolds stresses or turbulence heat fluxes.

3. Treatment of Reynolds stresses

3.1 Two-layer $k-\varepsilon$ model

In the most commonly used two-equation turbulence models the Reynolds stresses in Eq. (2) are modeled by the following Bousinesque assumption:

$$\overline{u_iu_j}=-\nu_T\left(\frac{\partial U_j}{\partial x_i}+\frac{\partial U_i}{\partial x_j}\right)+\frac{2}{3}k\delta_{ij} \tag{4}$$

where the turbulent eddy viscosity is given by

$$\nu_T=C_\mu\frac{k^2}{\varepsilon}. \tag{5}$$

The kinetic energy k and its dissipation rate ε in Eq. (5) is computed by the following partial differential equations:

$$\frac{D}{Dt}(k)=\frac{\partial}{\partial x_j}\left[\left(\nu+\frac{\nu_T}{\sigma_k}\right)\frac{\partial k}{\partial x_j}\right]+\left(P_k+G_k\right)-\varepsilon \tag{6}$$

$$\frac{D}{Dt}(\varepsilon)=\frac{\partial}{\partial x_j}\left[\left(\nu+\frac{\nu_T}{\sigma_\varepsilon}\right)\frac{\partial \varepsilon}{\partial x_j}\right]+\frac{\varepsilon}{k}\left[C_{\varepsilon 1}(P_k+G_k)-C_{\varepsilon 2}\varepsilon\right]. \tag{7}$$

In the two-layer model by Chen and Patel [4], the eddy viscosity and the rate of dissipation of turbulent kinetic energy in the near wall region are specified as follows employing the one-equation model:

$$\nu_T=C_\mu\sqrt{k}\,l_\mu,\quad \varepsilon=\frac{k^{3/2}}{l_\varepsilon} \tag{8}$$

where

$$l_\varepsilon=C_L y\left(1.-e^{-R_y/A_\varepsilon}\right),\quad l_\mu=C_L y\left(1.-e^{-R_y/A_\mu}\right)$$
$$R_y=y\rho\sqrt{k}/\mu. \tag{9}$$

In this model the equation of turbulence kinetic energy, Eq. (6), is solved all the way to the wall while the equation of the turbulence kinetic energy dissipation rate, Eq. (7), is solved in the outer region. It is noted that the length scales in Eq. (9) and constants in Eq. (9) is based on the forced convection turbulent boundary layer and it is questionable whether this model works well in the natural convection flows.

3.2 Elliptic relaxation (V2-f) model

In the elliptic relaxation model by Medic and Durbin [5] the governing equations for the turbulent kinetic energy (k) and its dissipation rate (ε) are the same as the $k-\varepsilon$ model except the expressions of the turbulent eddy viscosity and the time scale. The following two additional governing equations are solved to determine the velocity scale:

$$\frac{D}{Dt}(\rho\overline{v^2})=\frac{\partial}{\partial x_j}\left(\left(\mu+\frac{\mu_T}{\sigma_k}\right)\frac{\partial\overline{v^2}}{\partial x_j}\right)+\rho\left(kf-\frac{\varepsilon}{k}\overline{v^2}\right) \tag{10}$$

$$L_S^2\frac{\partial^2 f}{\partial x_j\partial x_j}-f=\frac{1}{T}\left(\left(C_1-1\right)\left(\frac{2}{3}-\frac{\overline{v^2}}{k}\right)\right)+C_2\frac{\left(P_k+G_k\right)}{k}. \tag{11}$$

In this model the turbulence eddy viscosity in Eq. (4) is given by

$$\nu_T=C_\mu\overline{v^2}T \tag{12}$$

and the time and length scales in the above equations are given by

$$T=\min\left(\max\left(\frac{k}{\varepsilon},C_T\left(\frac{\nu}{\varepsilon}\right)^{1/2}\right),\frac{\alpha k}{\sqrt{6}\overline{v^2}C_\mu|S|}\right) \tag{13}$$

$$L_S=C_L\max\left(\min\left(\frac{k^{3/2}}{\varepsilon},\frac{k^{3/2}}{\sqrt{6}\overline{v^2}C_\mu|S|}\right),C_\eta\left(\frac{\nu^3}{\varepsilon}\right)^{1/4}\right). \tag{14}$$

It is noted that the Reynolds stresses in this model are also based on the Bousinesque assumption given in Eq. (4).

3.3 Shear stress transport (SST) model

In the SST model by Menter [7] the governing equations for the k and ω are solved as follows:

$$\frac{D}{Dt}(\rho k)=\frac{\partial}{\partial x_j}\left[\left(\mu+\sigma_{k3}\mu_T\right)\frac{\partial k}{\partial x_j}\right]+\rho\left(P_k+G_k\right)-\beta^*\rho\omega k \tag{15}$$

$$\frac{D}{Dt}(\rho\omega)=\frac{\partial}{\partial x_j}\left[\left(\mu+\sigma_{\omega 3}\mu_T\right)\frac{\partial\omega}{\partial x_j}\right]+\rho\frac{\gamma_3}{\mu_T}(P_k+G_k)+2\rho(1-F_1)\frac{\sigma_{\omega 2}}{\omega}\frac{\partial k}{\partial x_j}\frac{\partial\omega}{\partial x_j}-\rho\beta_3\omega^2. \tag{16}$$

In this model the turbulence eddy viscosity in Eq. (4) is expressed by the following equation:

$$\nu_T=\frac{a_1 k}{\max(a_1\omega,SF_2)} \tag{17}$$

where

$$F_1=\tanh(\arg 1^4),\quad F_2=\tanh(\arg 2^2) \tag{18}$$

$$\arg 1=\min\left(\max\left(\frac{\sqrt{k}}{\beta^*\omega y},\frac{500\nu}{y^2\omega}\right),\frac{4\rho k\sigma_{\omega 2}}{CD_{k\omega}y^2}\right) \tag{19}$$

$$\arg 2=\max\left(\frac{2\sqrt{k}}{\beta^*\omega y},\frac{500\nu}{y^2\omega}\right) \tag{20}$$

$$CD_{k\omega}=\max\left(\frac{2\rho\sigma_{\omega 2}}{\omega}\frac{\partial k}{\partial x_j}\frac{\partial\omega}{\partial x_j},10^{-10}\right). \tag{21}$$

The coefficient of SST model are a linear combination of the corresponding coefficients such that

$$\Phi_3=F_1\Phi_1+(1-F_1)\Phi_2 \tag{22}$$

where F_1 is a blending function defined by Eq. (18), and the σ_{k3}, $\sigma_{\omega 3}$, β_3, and γ_3 are calculated by Eq. (22). This model is also based on the Bousinesque assumption, Eq. (4), in the expression of the Reynolds stresses.

3.4 Differential stress model

In the elliptic-blending second-moment closure by Thielen et al. [8], the Reynolds stresses in Eq. (2) are obtained through the solution of the following partial differential equations:

$$\frac{D}{Dt}(\rho\overline{u_iu_j}) = \frac{\partial}{\partial x_k}\left[\left(\mu\delta_{kl} + C_s\,\rho\,\overline{u_ku_l}\,T\right)\frac{\partial\overline{u_iu_j}}{\partial x_l}\right] + \rho\left(P_{ij} + G_{ij} + \Phi_{ij} - \varepsilon_{ij}\right) \tag{23}$$

where

$$P_{ij} = -\overline{u_iu_k}\frac{\partial U_j}{\partial x_k} - \overline{u_ju_k}\frac{\partial U_i}{\partial x_k} \tag{24}$$

$$G_{ij} = -g_i\beta\overline{u_j\theta} - g_j\beta\overline{u_i\theta} \tag{25}$$

$$\Phi_{ij} = (1-\alpha^2)\Phi_{ij}^w + \alpha^2\Phi_{ij}^h \tag{26}$$

$$\Phi_{ij}^h = -\left(C_1 + C_2\frac{P_k}{\varepsilon}\right)\varepsilon\,A_{ij} + C_3kS_{ij} + C_4k\left(A_{ik}S_{jk} + A_{jk}S_{ik} - \frac{2}{3}\delta_{ij}A_{lk}S_{kl}\right) + C_5k\left(A_{ik}\Omega_{jk} + A_{jk}\Omega_{ik}\right) - C_6(G_{ij} - \frac{2}{3}G_K\delta_{ij}) \tag{27}$$

$$\Phi_{ij}^w = -5\frac{\varepsilon}{k}\left(\overline{u_iu_k}n_jn_k + \overline{u_ju_k}n_in_k - \frac{1}{2}C_1\overline{u_ku_l}n_kn_l\left(n_in_j + \delta_{ij}\right)\right) \tag{28}$$

$$\varepsilon_{ij} = (1-\alpha^2)\frac{\overline{u_iu_j}}{k}\varepsilon + \frac{2}{3}\alpha^2\varepsilon\delta_{ij} \tag{29}$$

$$\alpha - L^2\frac{\partial^2\alpha}{\partial x_j\partial x_j} = 1\,,\quad n = \frac{\nabla\alpha}{\|\nabla\alpha\|}\,. \tag{30}$$

It is noted that this model is free from the wall related parameters, which facilitate implementation of this model in complex geometries.

4. Treatment of turbulent heat fluxes

4.1 Simple gradient diffusion hypothesis (SGDH)

In the SGDH, the turbulent heat fluxes ($\overline{\theta u_j}$) in Eq. (3) are treated by the following equation:

$$\overline{\theta u_i} = -\frac{\nu_t}{\mathrm{Pr}_t}\frac{\partial\Theta}{\partial x_i}\,. \tag{31}$$

In this equation Pr_t is the turbulent Prandtl number. It is well known that this assumption is not adequate for natural convection flows although it is widely used in forced convection flows. Thus, this assumption is not considered in the present study.

3.2 Generalized gradient diffusion hypothesis (GGDH)

In the GGDH by Ince and Launder [11], the turbulent heat fluxes ($\overline{\theta u_j}$) in Eq. (3) are approximated by the following equation.

$$\overline{\theta u_i} = -C_\theta\frac{k}{\varepsilon}\left(\overline{u_iu_k}\frac{\partial\Theta}{\partial x_k}\right) \tag{32}$$

As shown in the above equation, the accuracy of this assumption depends on the accuracy of the computed Reynolds stresses. Ince and Launder [11] and Choi and Kim [9] used the GGDH for natural convection in a rectangular cavity with success. However, it is known that this assumption is not adequate for a natural convection with a strong stratification.

3.3 Algebraic flux model (AFM)

In the AFM by Kenjeres and Hanjalic [12] the turbulent heat fluxes are computed by the following algebraic equation:

$$\overline{\theta u_i} = -C_\theta\frac{k}{\varepsilon}\left(\overline{u_iu_j}\frac{\partial\Theta}{\partial x_j} + \xi\overline{\theta u_j}\frac{\partial U_i}{\partial x_j} + \eta\beta g_i\overline{\theta^2}\right). \tag{33}$$

When compared with the GGDH model, the last term with a temperature variance has a positive effect on the gravitational generation term G_k and it prevents G_k from being negative value. This effect stabilizes the overall solution process, especially for strongly stratified flows.

3.4 Differential flux model (DFM)

Shin et al. [16] proposed the following differential equations for the turbulent heat fluxes.

$$\frac{D}{Dt}(\rho\overline{u_i\theta}) = \frac{\partial}{\partial x_k}\left[\left(\frac{1}{2}(\mu + \frac{\mu}{\mathrm{Pr}})\delta_{kl} + C_\theta\,\rho\,\overline{u_ku_l}\,T\right)\frac{\partial\overline{u_i\theta}}{\partial x_l}\right] + \rho(P_{i\theta} + G_{i\theta} + \Phi_{i\theta}^* - \varepsilon_{i\theta}) \tag{34}$$

where

$$P_{i\theta} = -\overline{u_iu_k}\frac{\partial\Theta}{\partial x_k} - \overline{u_k\theta}\frac{\partial U_i}{\partial x_k} \tag{35}$$

$$G_{i\theta} = -g_i\beta\overline{\theta^2} \tag{36}$$

$$\Phi_{i\theta}^* = (1-\alpha^2)\Phi_{i\theta}^w + \alpha^2\Phi_{i\theta}^h \tag{37}$$

$$\varepsilon_{i\theta} = (1-\alpha^2)\varepsilon_{i\theta}^w + \alpha^2\varepsilon_{i\theta}^h \tag{38}$$

$$\Phi_{i\theta}^h = -C_{1\theta}\frac{\varepsilon}{k}\overline{u_i\theta} + C_{2\theta}\overline{u_j\theta}\frac{\partial U_i}{\partial x_j} + C_{3\theta}g_i\beta\overline{\theta^2} \tag{39}$$

$$\Phi_{i\theta}^w = -\frac{\varepsilon}{k}\overline{u_k\theta}\;n_kn_i \tag{40}$$

$$\varepsilon_{i\theta}^h = 0.\,,\quad \varepsilon_{i\theta}^w = \frac{1}{2}(1+\frac{1}{\mathrm{Pr}})\frac{\varepsilon}{k}(\overline{u_i\theta} + \overline{u_k\theta}\;n_kn_i)\,. \tag{41}$$

This model is a thermal version of the elliptic-blending sec-

ond-moment closure by Thielen et al. [8]. The model is simple to implement and is free from the wall-related parameters.

5. Numerical methods

The turbulence models considered in the present study are implemented in a computer code especially designed for the evaluation of turbulence models. The computer code employs the non-staggered grid arrangement and the SIMPLE algorithm by Patankar [17] for the pressure-velocity coupling. The second-order bounded HLPA scheme by Zhu [18] is used for treating the convection terms for all the computed variables.

6. Results and discussion

6.1 Natural convection in a rectangular cavity

The first test problem considered in the present study is a natural convection of air in a rectangular cavity with an aspect ratio of 1:5 as shown in Fig. 1. The height of the cavity is $H = 2.5m$, the width of the cavity is $L = 0.5m$ and the temperature difference between the hot and cold walls is 45.8°K. The Rayleigh number based on the height of the cavity is $Ra = 4.3 \times 10^{10}$ and the Prandtl number is $\Pr = 0.71$. King [10] has carried out extensive measurements for this problem and his experimental data is reported in King [10] and Cheesewright et al. [19]. The experimental data by King [10] contains a problem in that the top wall is not fully insulated. This makes the turbulence level near the hot wall high and that near the cold wall low, and this affects the distribution of the turbulence quantities in all the solution domain. Such a deficiency will be shown clearly for the distribution of the Reynolds shear stress at y/H=0.5. This experimental data is employed here to investigate the effect of different treatments of Reynolds stresses and turbulence heat fluxes on the solution.

We first investigate how the different treatment of Reynolds stress effects the accuracy of solution when the turbulence heat fluxes are treated by the same algebraic flux model (AFM). Figs. 2 shows the comparison of the predicted results with the measured data by Cheesewright et al. [19] for the vertical velocity component at y/H=0.5. As shown in the figures, the agreement between the measured data and the predictions by the V2-f, SMC-DH and EBM models is fairly good although there exist small differences. The SMC-DH means the second moment closure used by Dol and Hanjalic [14] and Choi et al. [15]. The prediction by the two-layer model is significantly different from the measured data. This model produces a laminar-like solution in the near wall region. As mentioned before, it is due to the fact the length scales and constants in Eq. (9) is based on the forced convection turbulent boundary layer and this model does not work well in the natural convection flows.

Fig. 3 shows the comparison of the predicted vertical velocity fluctuation at the mid-height (y/H=0.5) with the experi-

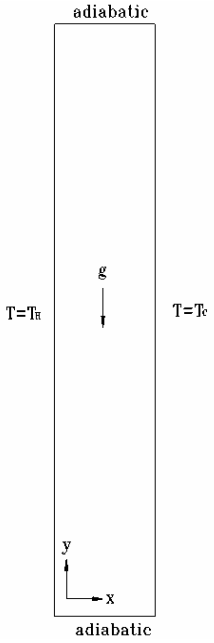

Fig. 1. A schematic picture of the 5:1 rectangular cavity.

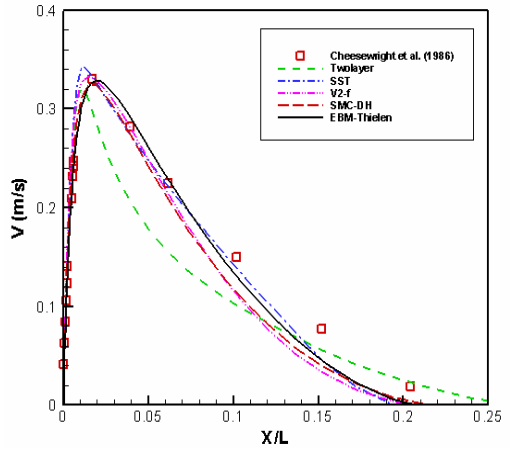

(a) Near the hot wall

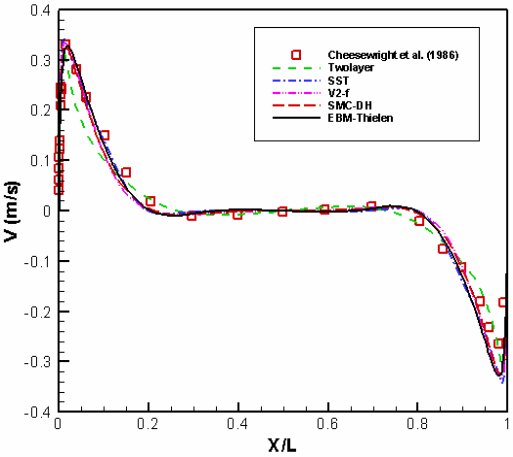

(b) Total view

Fig. 2. Mean vertical velocity profiles at y/H=0.5.

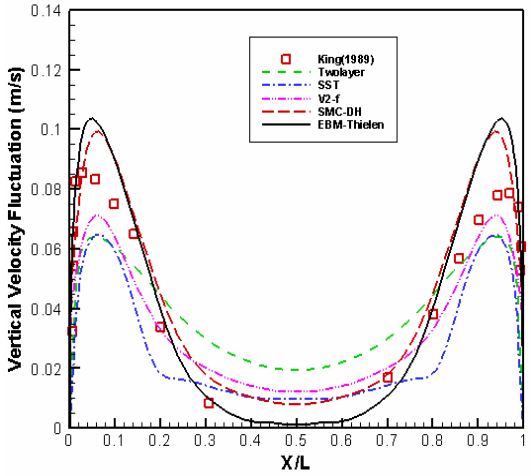

Fig. 3. Vertical velocity fluctuation profiles at y/H=0.5.

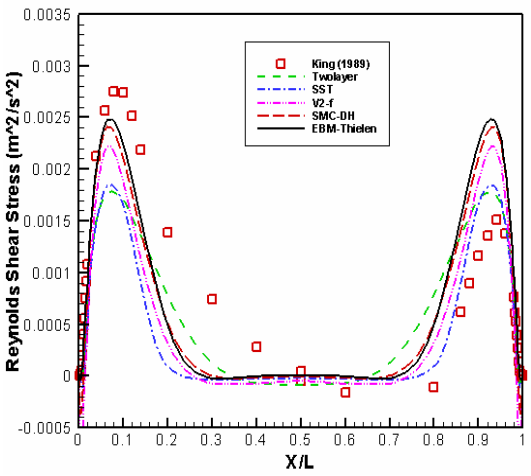

Fig. 4. Reynolds shear stress profiles at y/H=0.5.

mental data. The SMC-DH and EBM models slightly over-predict it and the V2-f and SST models under-predict it in the near wall region. The two-layer model under-predicts it in the near wall region and over-predicts it at the edge of the boundary layer. This is due to the fact that the flow from the edge of the boundary layer to the core is quiescent and thermally stratified and the conventional $k-\varepsilon$ model, which can not handle a low level turbulence properly, is used to compute the flow and thermal fields in this region in the two-layer model. The rather poor predictions by the V2-f, SST and two-layer models may be partly due to the use of the Bussinesq assumption to compute the vertical velocity fluctuation. The prediction by the EBM follows the trend of the measured data best.

Fig. 4 shows the profiles of the predicted Reynolds shear stress $\overline{uv}$ at the mid-plane (y/H=0.5) of the cavity together with the measured data. The EBM, SMC-DH and V2-f models slightly under-predict the $\overline{uv}$ near the hot wall and over-predict it near the cold wall when compared with the experimental data. As explained before, it is due to the insufficient insulation of the top wall in the experiment. The performances of the EBM, SMC-DH and V2-f models for prediction of $\overline{uv}$ are nearly the same, and the two-layer and SST models behave similarly and they under-predict $\overline{uv}$.

Figs. 5 show the profiles of the predicted turbulent heat fluxes, $\overline{\theta v}$ and $\overline{\theta u}$, at the mid-plane (y/H=0.5) of the cavity with the measured data. It is noted that the vertical turbulent heat flux vector $\overline{\theta v}$ plays a very important role in the dynamics of the turbulent kinetic energy in the buoyant turbulent flows and it influences directly the overall prediction of all the quantities. The AFM used in the present study for the two-layer, SST and V2-f models, contains all the temperature and mean velocity gradients together with the correlation between the gravity vector and temperature variance. All the models predict well the vertical turbulent heat flux and the V2-f and SMC-DH models slightly under-predict the vertical turbulent heat flux $\overline{\theta v}$ near the hot wall and the peak regions of $\overline{\theta v}$ are skewed a little toward the center region as shown in Fig.

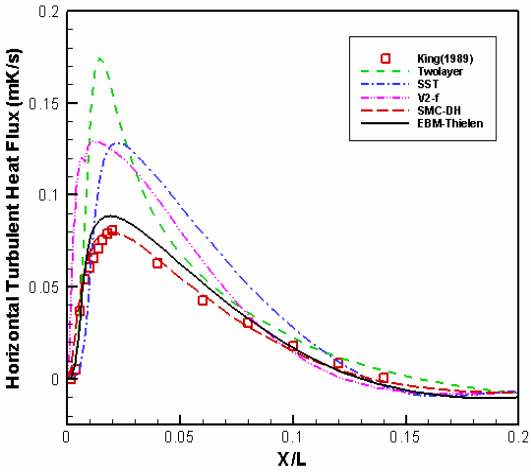

(a) Horizontal turbulent heat flux $\overline{\theta u}$

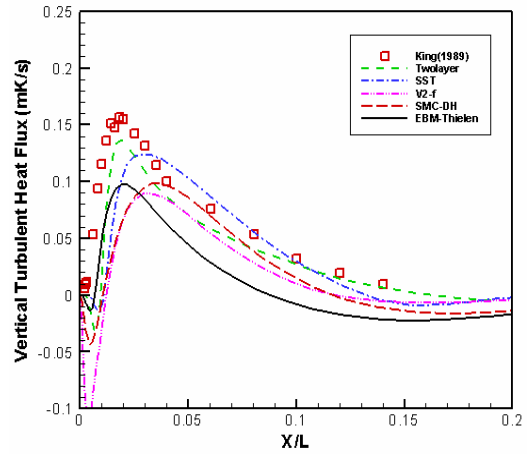

(b) Vertical turbulent heat flux $\overline{\theta v}$

Fig. 5. Turbulent heat fluxes profiles at y/H=0.5.

5(b). The two-layer model predicts well the vertical turbulent heat flux near the hot wall region and the peak regions are

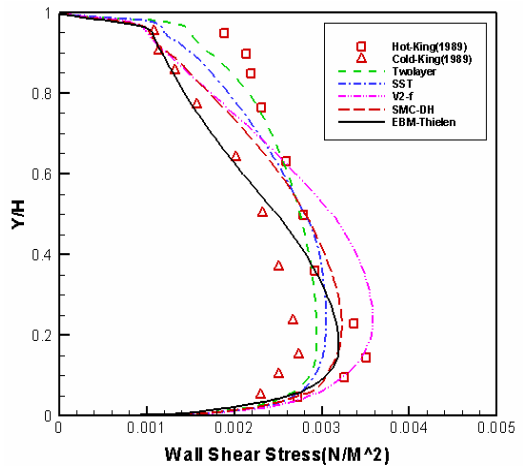

Fig. 6. Wall shear stress distribution along the vertical wall.

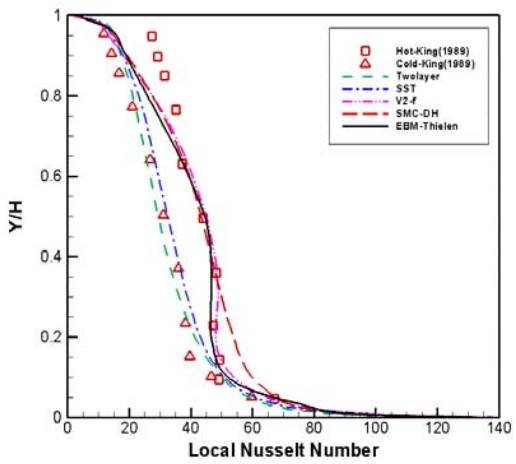

Fig. 7. Local Nusselt number distribution along the vertical wall.

skewed to the hot wall, but the shape of the predicted profile is a little thin when compared with the other predictions. The EBM model under-predicts the vertical turbulent heat flux, however, the shape of the predicted vertical turbulent heat flux by this model follows the trend of the experimental data. Fig. 5(a) shows that the SMC-PH and EBM models predict very accurately the horizontal turbulent heat flux $\overline{\theta u}$, while the other models over-predict it severely. This fact shows that the AFM which is used with the EBM model predicts the turbulent heat flux well when the turbulent stresses are predicted accurately.

Fig. 6 shows the comparison of the predicted results with the measured data for the wall shear stress at the hot wall reported in King [10]. We observe that V2-f model predicts the peak value of the wall shear stress at the hot wall well, but it over-predicts the wall shear stress after the peak region. The trend of the prediction of the wall shear stress by the SMC-DH model is nearly the same as that by the V2-f model and the SMC-DH model slightly under-predicts the peak value of the wall shear stress. The trend of the prediction by the two-layer and SST model is different from that by the V2-f and SMC-DH models. We can observe that even the V2-f and SMC-DH models do not predict well the laminar to turbulent transition at the hot wall observed in the experimental data. It is noted that the measurement of the velocity components near the bottom wall is more accurate than that near the top wall due to an insufficient insulation at the top wall. The EBM model predicts the wall shear stress best.

Fig. 7 shows the comparison of the predicted results with the measured data for the local Nusselt number at the hot wall reported in King [10]. The V2-f model predicts accurately the local Nusselt number at the hot wall, and the transition phenomenon at the lower portion of the hot wall is also predicted well. The SMC-DH model predicts well the local Nusselt number at the hot wall, however, it does not predict the laminar to turbulent transition observed in the experimental data. The two-layer and SST models predict the local Nusselt number at the hot wall poorly and they do not predict the transition

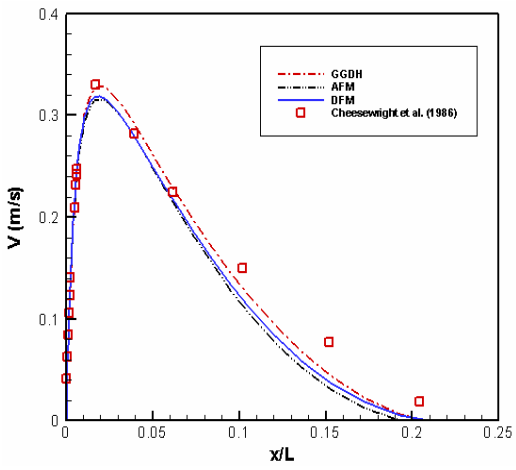

(a) Near the hot wall

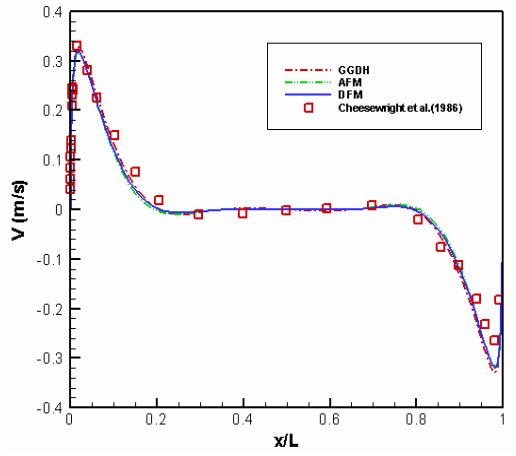

(b) Total view

Fig. 8. Mean vertical velocity profiles at y/H=0.5.

phenomenon. The V2-f model predicts the local Nusselt number well and its prediction is as accurate as the EBM.

From here the effect of different treatment of turbulence

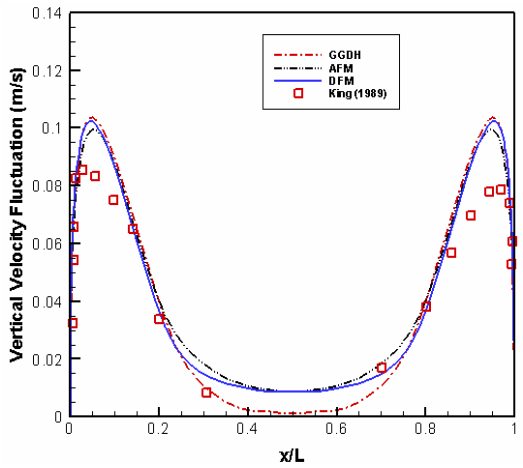

Fig. 9. Vertical velocity fluctuation profiles at y/H=0.5.

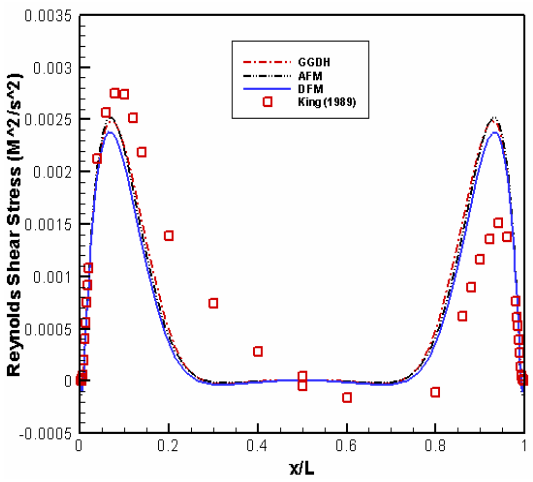

Fig. 10. Reynolds shear stress profiles at y/H=0.5.

heat fluxes on the solution while the Reynolds stresses are treated by the EBM is investigated. Fig. 8 shows the comparison of the predicted results with the measured data for the vertical velocity component at y/H=0.5. As shown in the figures, the agreement between the measured data and the predictions by the GGDH, AFM and DFM models are fairly good although a small difference exists. This figure shows that the GGDH model predicts the mean vertical velocity fairly well for this simple shear dominant flow without a strong stratification.

Fig. 9 shows the comparison of the predicted vertical velocity fluctuation at a mid-height (y/H=0.5) with the experimental data. The GGDH, AFM and DFM over-predict it in the near wall region. The experimental data shows a symmetric profile, however, when one considers the insufficient insulation problem at the top wall, the profile near the hot wall is not a correct one. Therefore, the magnitude of the experimental data near the hot wall should be greater than that near the cold wall. We observed that the predictions follow the trend of the measured data well except for the central region of the cavity where the flow is weakly stratified. The prediction by GGDH shows that the vertical velocity fluctuation is nearly zero at the central region of the cavity even in this weakly stratified region, while AFM and DFM avoid this problem. As mentioned before, it is due to the fact that a gravity term with a temperature variance exists in the algebraic (AFM) or differential (DFM) formulations of the turbulent heat fluxes. We can conjecture that the GGDH model may invoke a numerical stability problem when it is applied to flows with a strong stratification. Fig. 10 shows the profiles of the predicted Reynolds shear stress $\overline{uv}$ at a mid-plane (y/H=0.5) of the cavity together with the measured data. The GGDH, AFM and DFM models slightly under-predict the $\overline{uv}$ near the hot wall and over-predict it near the cold wall due to the insufficient insulation problem at the top wall. The performances of the three models for the prediction of $\overline{uv}$ are nearly the same.

Fig. 11 shows the profiles of the predicted horizontal and vertical turbulent heat fluxes, $\overline{\theta v}$ and $\overline{\theta u}$, at a mid-plane (y/H=0.5) of the cavity with the measured data. It is noted that

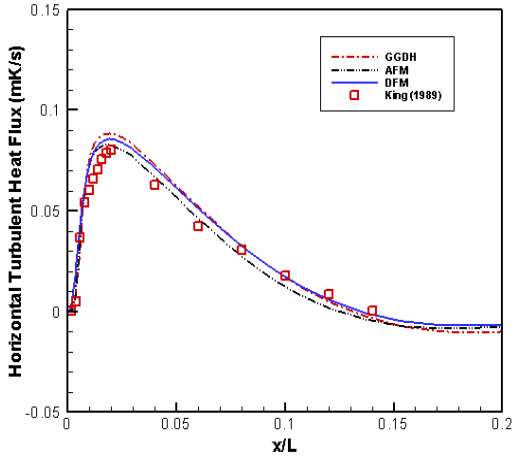

(a) Horizontal turbulent heat flux $\overline{\theta u}$

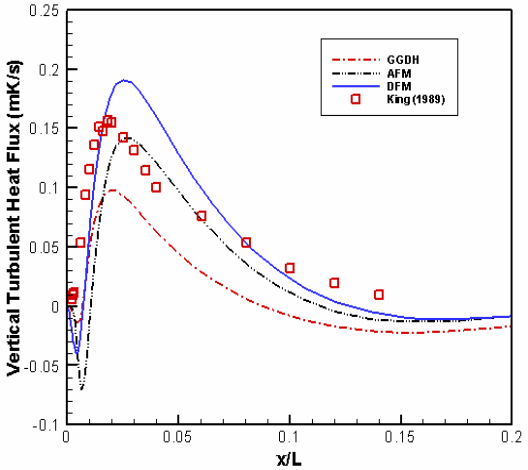

(b) Vertical turbulent heat flux $\overline{\theta v}$

Fig. 11. Turbulent heat fluxes profiles at y/H=0.5.

the AFM and DFM contain all the temperature and mean velocity gradients together with a correlation between the gravity vector and temperature variance. The three models predict the

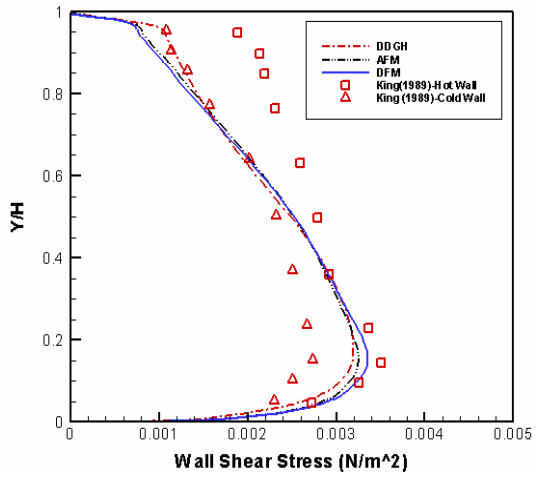

Fig. 12. Wall shear stress distribution along the vertical wall.

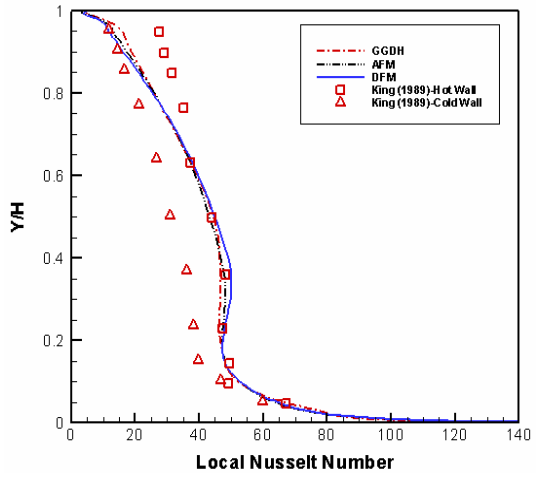

Fig. 13. Local Nusselt number distribution along the vertical wall.

horizontal turbulent heat flux $\overline{\theta u}$ fairly well. The GGDH model under-predicts the vertical turbulent heat flux $\overline{\theta v}$ near the hot wall while the DFM slightly over-predicts it. The AFM predicts best the vertical turbulent heat flux near the hot wall region.

Fig. 12 and Fig. 13 show the comparisons of the predicted results with the measured data for the wall shear stress and the local Nusselt number at the hot wall, reported in King [10]. The three models predict the wall shear stress and local Nusselt number at the hot wall very well and the smooth laminar to turbulent transition at the lower portion of the hot wall observed in the experimental data is also predicted well.

6.2 Natural convection in a square cavity with conducting walls

The second test problem is the experiment conducted by Ampofo and Karayiannis [20]. This test problem is a natural convection of air in a square cavity with two isothermal side

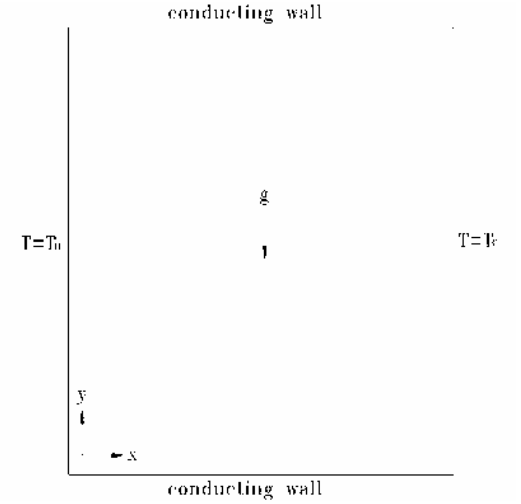

Fig. 14. A schematic picture of the square cavity with conducting walls.

walls and two conducting walls at the top and bottom as shown in Fig. 14. The height of the cavity is $H = 0.75m$ and the temperature difference between the hot and cold walls is 40 ^{o}K. The Rayleigh number based on the height of the cavity is $Ra = 1.58 \times 10^{9}$ and the Prandtl number is $\Pr = 0.71$. The detailed experimental data is tabulated in Ampofo and Karayinnis [20]. The top and bottom walls are conducting walls and the boundary conditions for the temperature for these walls are specified by using the data given in Ampofo and Karayinnis [20]. The experiment conducted by Ampofo and Karayiannis [20] for a square cavity is the most challenging case for an evaluation of turbulence models. The LES solution by Peng and Davidson [21] is available for this flow and it is compared with the present predictions. The turbulence level in the central region is very low, and the flow is stagnant and thermally stratified. The boundary layer is thin and the turbulence intensity level is low. Thus, this experiment is a good test problem for investigating the effect of different treatment of turbulence heat fluxes on the accuracy of solution.

We first compared the predicted results with the measured data reported in Ampofo and Karayinnis [20] for the vertical mean velocity. Fig. 15 show the comparisons of the predicted results with the measured data for the vertical velocity component at a mid-height (y/H=0.5) of the cavity. As shown in the figure, the agreement between the measured data and the predictions by the AFM and DFM models is very good and follows the trend of the measured data. However, we can observe that the solution by the GGDH model looks like laminar solution and deviates much from the experimental data. As shown before, Choi and Kim [9] predicts accurate solutions for a simple shear dominant flow within the 1:5 rectangular cavity using the GGDH model, however, this model predicts a very poor solution or invokes a numerical oscillation when applied to a flow with a relatively strong stratification like the present problem. Due to this reason we did not perform an adjustment of the turbulence model constants for the GGDH

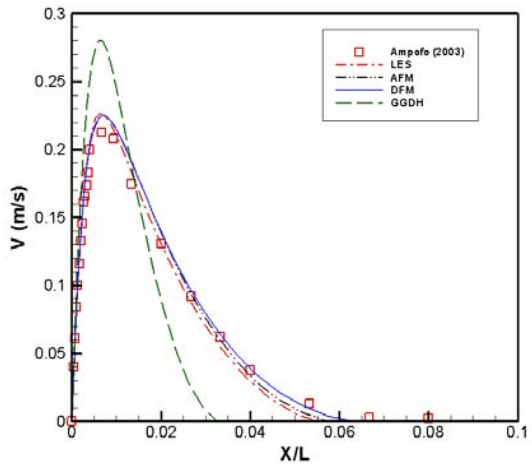

(a) Near the hot wall

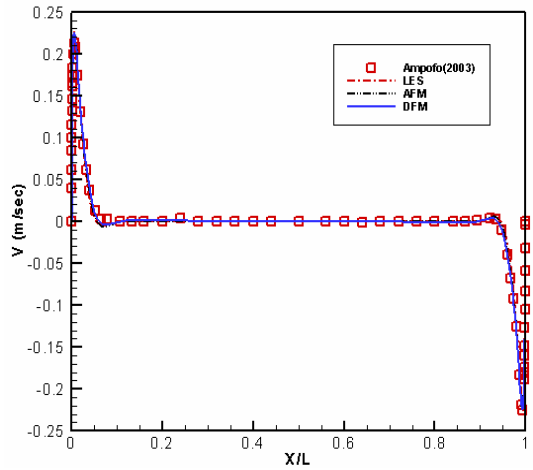

(b) Total view

Fig. 15. Mean vertical velocity profiles at y/H=0.5.

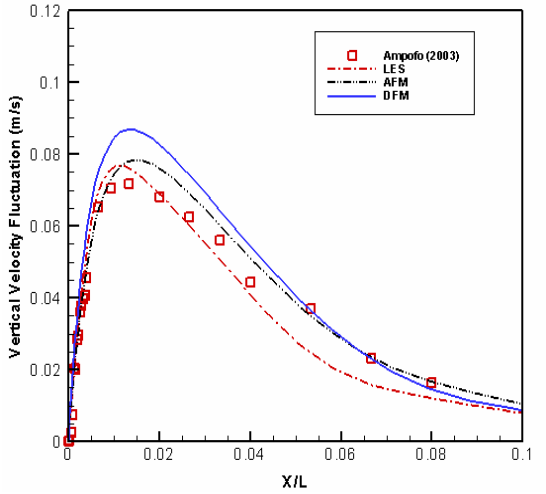

(a) Vertical velocity fluctuation

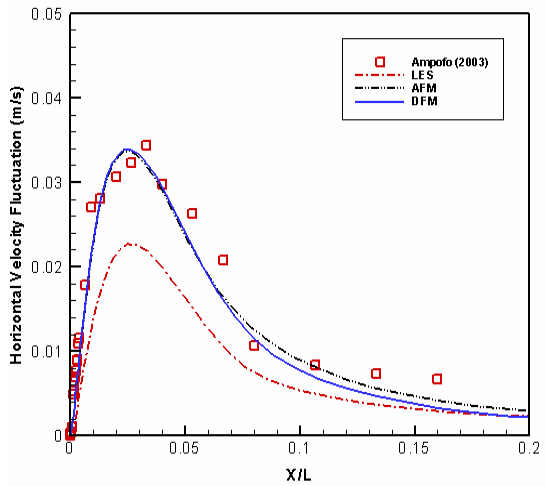

(b) Horizontal velocity fluctuation

Fig. 16. Vertical and horizontal velocity fluctuation profiles at y/H=0.5.

for this problem. We can observe that the predictions by the AFM and DFM turbulence models are as good as the LES solution.

Figs. 16 and 17 show the comparisons of the predicted results with the measured data for the turbulent quantities such as the horizontal and vertical velocity fluctuations and the Reynolds shear stress at a vertical mid-plane of the cavity (y/H=0.5). Figs. 16 and 17 show that the predictions by the AFM and DFM agree well with the measured data although the DFM slightly over-predicts the vertical velocity fluctuation. It is not understood why the LES calculation by Peng and Davidson [21] under-predicts the turbulent quantities.

Fig. 18 shows the comparisons of the predicted results with the measured data for the mean temperature at a mid-height (y/H=0.5) of the cavity. No real differences among the models for the horizontal temperature distribution at a mid-plane (y/H=0.5) exist, while the LES predicts it accurately.

Fig. 19 shows the predicted results for the local Nusselt number at the hot and bottom walls together with the meas-

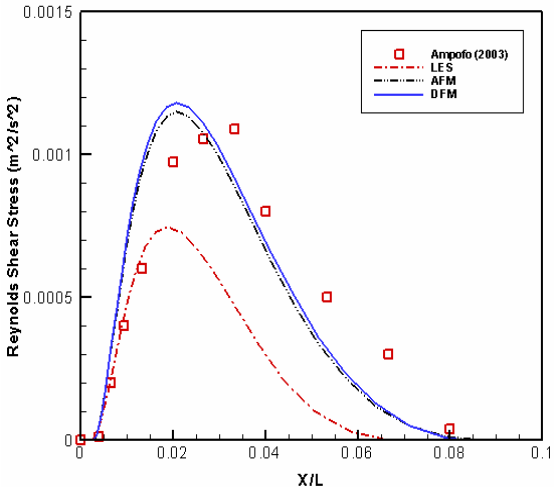

Fig. 17. Reynolds shear stress $\overline{uv}$ profiles at y/H=0.5.

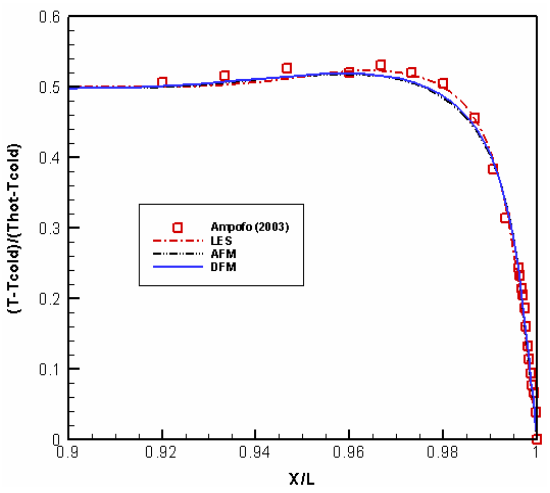

Fig. 18. Horizontal centerline temperature profiles at y/H=0.5.

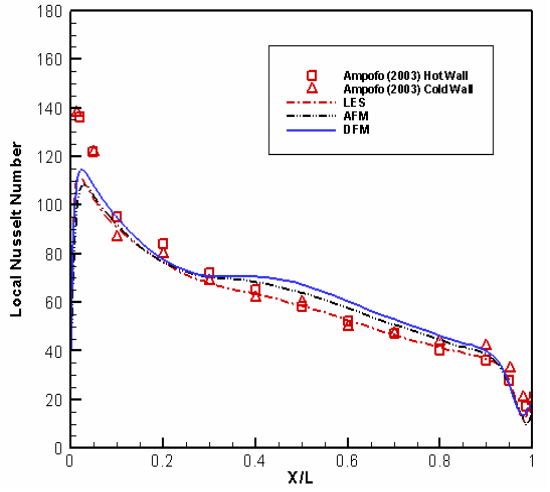

(a) Hot wall

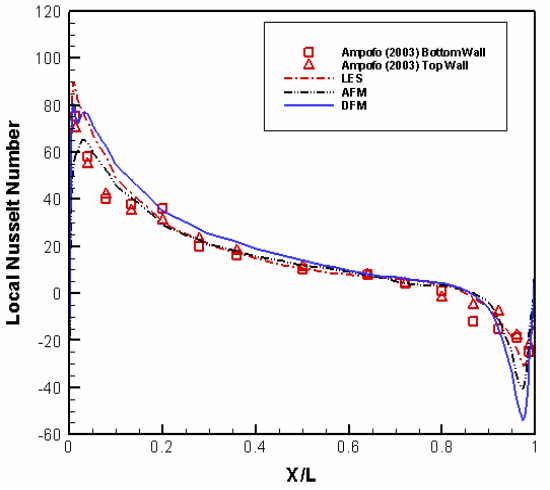

(b) Bottom wall

Fig. 19. Local Nusselt number distributions along the hot and bottom walls.

ured data. It is observed that the DFM model slightly over-predicts the local Nusselt number at the hot and bottom walls, while the AFM rather accurately predicts the local Nusselt number at the hot and bottom walls. It is noted that the predictions of the local Nusselt number at the hot wall by the AFM and DFM show a smooth transition which was not observed in the experimental data and LES solution. The AFM predicts the Nusselt number as accurately as the LES solution.

6.3 Rayleigh-Benard convection

The Rayleigh-Benard convection is the flow between two walls heated at the bottom and cooled at the top. Due to the importance of this flow in industrial and environmental applications, a number of works are reported in the literatures, and Kenjeres [22] summarized most of the previous experimental and numerical works. The Rayleigh-Benard convection is characterized by a large cellular motion. When the Rayleigh number is relatively small, this cellular motion is clearly observed from experiments or numerical calculations. When the Rayleigh number is large, the heat transfer near the bottom and top walls occurs at a very thin boundary layer near the wall and a very large number of grids are required for an accurate prediction of such a flow. Most of the recent works in the literatures employ the DNS (direct numerical simulation) or LES (large eddy simulation) approaches and their solutions are limited to the low-Rayleigh number region. Since detailed information of a flow cannot be provided for high-Rayleigh number flows, most authors have devoted their efforts to finding the Nusselt and Rayleigh number relation ($Nu \approx cRa^a \Pr^b$) for an overall heat transfer.

The RANS (Reynolds averaged Navier-Stokes) equation approach for the Rayleigh-Benard convection, which can be applied to high-Rayleigh number flows, is limited and has been done mainly by Kenjeres and Hanjalic [23-26] within the present author's knowledge. These authors used a two-equation, low-Reynolds number algebraic $k-\underline{\varepsilon}-\theta^2-\varepsilon_\theta$ model in which the temperature variance term (θ^2) and the molecular dissipation of a turbulent heat flux (ε_θ) is included in the expression of the turbulent heat fluxes. In the present study the elliptic-blending model is applied to the simulation of a turbulent Rayleigh-Benard convection.

The primary emphasis of the present study is placed on how the elliptic-blending second-moment closure with an algebraic flux model works for a turbulent Rayleigh-Benard convection. Calculations are performed for six different Rayleigh numbers and the computed results are compared with available experimental data and previous numerical results.

In the present study, the turbulent heat fluxes ($\overline{\theta u_i}$) in Eq. (3) are given by the algebraic flux model [25];

$$\overline{\theta u_i} = -C_\theta T\left(\overline{u_i u_k}\frac{\partial \Theta}{\partial x_k} + \xi\overline{\theta u_k}\frac{\partial U_i}{\partial x_k} + \eta\beta g_i\overline{\theta^2} + \varepsilon_{\theta i}\right) \quad (42)$$

(a) Velocity vector for $Ra = 10^7$

(b) Streamlines for $Ra = 10^7$

(c) Velocity vector for $Ra = 10^9$

(d) Streamlines for $Ra = 10^9$

Fig. 20. The predicted velocity vectors and streamlines for $Ra = 10^7$ and $Ra = 10^9$.

$$\varepsilon_{\theta i} = f_{\varepsilon\theta i}\frac{1+\mathrm{Pr}}{2\sqrt{\mathrm{Pr}R}}\frac{\varepsilon}{k}\overline{\theta u_i},\ f_{\varepsilon\theta i} = \exp[-C_{c\varepsilon\theta i}\,\mathrm{Re}_t(1+\mathrm{Pr})],$$
$$\mathrm{Re}_t = \frac{k^2}{\nu\varepsilon} \tag{43}$$

As a typical case of a Rayleigh-Benard convection, we consider a natural convection within an enclosure of a 8:1 aspect ratio where the bottom wall is heated and the upper wall is cooled. A symmetry condition is imposed at the lateral boundaries to mimic the infinite horizontal boundaries. The 82 non-uniform grids are generated in the vertical direction and the smallest grid size near the walls is $\Delta y/H = 4\times10^{-4}$ where H is the vertical distance between two horizontal walls. In the lateral direction 127 uniform grids are generated. Calculations are performed for six different Rayleigh numbers, 2×10^6, 10^7, 4×10^7, 10^8, 5×10^8 and 10^9.

Fig. 20 shows the predicted velocity vectors and streamlines for $Ra = 10^7$ and $Ra = 10^9$ respectively. We can observe that the number of rolls is nine when $Ra = 10^7$ and it is seven when $Ra = 10^9$. One roll exists at the center and the other rolls are symmetric with respect to the center roll, and the number of rolls is an odd number for both cases. In the calculations by Kenjeres and Hanjalic [23] the number of rolls was an even number for all the case considered. In their calculation six rolls were predicted when $Ra = 10^7$ and the rolls were symmetric with respect to the centerline. In our experiences, the formation of the roll structures depends on the numerical method, initial and boundary conditions and the Rayleigh number. Thus, a concrete conclusion for this phenomenon cannot be drawn here. Like in the previous calculations [23], the size of the roll increases with an increase of the Rayleigh number.

Fig. 21 shows the predicted local Nusselt number distributions at the hot and cold walls for $Ra = 10^7$ and $Ra = 10^9$ respectively. The organized roll structure causes a strong variation of the local Nusselt number at the hot and cold walls. The amplitude and wave length of the distribution of the local Nusselt number relate closely with the roll structure. As is clearly shown in the figures, the maximum value of the local Nusselt is located at the point where the plume impinges on the wall, while the minimum value of the local Nusselt is located at the position where the plume is released from the wall. We can also observe that the amplitude and wave length of the local Nusselt number increase with an increasing Rayleigh number, thus the roll become more elongated in the horizontal direction and the amplitude becomes larger as the Rayleigh number increases. A sharper variation of the local Nusselt number occurs at the impinging point when the Rayleigh number is larger ($Ra = 10^9$). The shape of the local Nusselt number at the position where the plume is released from the wall becomes duller with an increase of the Rayleigh number.

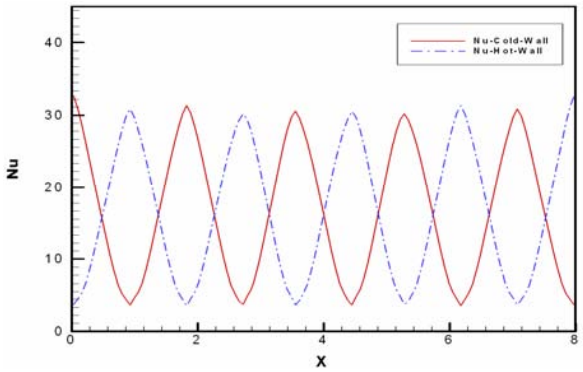

(a) $Ra = 10^7$

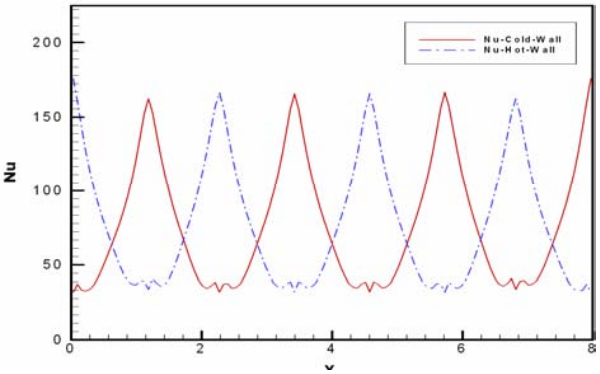

(a) $Ra = 10^9$

Fig. 21. The predicted local Nusselt number for $Ra = 10^7$ and $Ra = 10^9$.

It is very difficult to compare our results with other DNS, LES and experimental data since no detailed experimental or DNS data are available for a higher Rayleigh number region. The only way for a validation of the computation can be made by comparing the long term averaged Nu numbers with experimental correlations. However, many contradictions exist regarding the Nusselt number versus Rayleigh and Prandtl number relation ($Nu \approx cRa^a\,\mathrm{Pr}^b$). Many correlations by DNS,

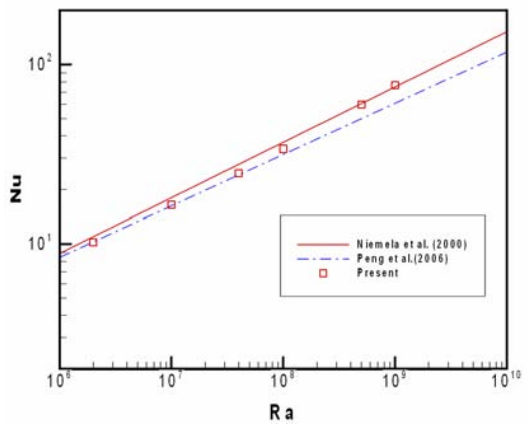

Fig. 22. The predicted overall Nusselt number versus Rayleigh number with the LES results and the experimental correlation.

LES and experiments have been proposed in the past and the results of these studies are summarized well in Kenjeres [22] and Kenjeres and Hanjalic [23]. In the earlier studies the relation $Nu \approx Ra^{1/3}$ was proposed, however, Wu and Libchaber [27] and another Chicago group claimed that such a correlation only works for a low-Rayleigh number region. This scaling region ($Ra \le 4\times10^7$) is called a 'soft' convective turbulence region and a higher Rayleigh number region ($Ra \ge 4\times10^7$) is called a 'hard' convective turbulence region. Most of the previous authors developed a single correlation that covers 'soft' and 'hard' convective turbulence regions. Fig. 22 shows the present results for the overall Nusselt number versus Rayleigh number together with the correlation by the LES results from Peng et al. [28] ($Nu = 0.162Ra^{0.286}$) and the experimental correlation by Niemela et al. [29] ($Nu = 0.124Ra^{0.309}$). This figure shows that our results follow with the correlation by Peng et al. [28] in the 'soft' convective turbulence region ($Ra \le 4\times10^7$) well, and at the transition point ($Ra \approx 4\times10^7$), the simulation results begin to deviate from the correlation by Peng et al. [28], and after a certain transition region around $Ra \approx 10^8$, it follows the correlation by Niemela et al. [29] at the 'hard' convective turbulence region ($10^8 \le Ra \le 10^9$). Within the present author's knowledge, nobody has reported a numerical simulation or experimental correlation that shows this trend. The fine grid ($256\times128\times256$) LES solution by Kenjeres and Hanjalic [25] matches very well with the present results for Rayleigh numbers ranging $10^8 \le Ra \le 10^9$. It is unfortunate that they did not carry out calculations for Rayleigh number less than $Ra \approx 10^7$. It is worth while mentioning that the two-dimensional prediction by Kenjeres and Hanjalic [23] follows the experimental correlation by Niemela et al. [29], even in the 'soft' convective turbulence region. They used a modified version of the low-Reynolds number $k-\varepsilon$ model by Launder and Sharma [3]. As shown in Fig. 20 the flow involves more impinging regions in the 'soft' convective turbulence region and it is well known that the $k-\varepsilon$ turbulence model predicts an excessively high turbulence kinetic energy in an impinging stagnation region. It is our conjecture that their over-prediction of the Nusselt number in the 'soft' convective turbulence region may be due to this stagnation anomaly of the $k-\varepsilon$ turbulence model. When the Rayleigh number becomes higher, the impinging region becomes smaller. Then, the effect of the stagnation anomaly of the $k-\varepsilon$ turbulence model becomes smaller, and thus, their results closely match with our results. It is noted that the elliptic-blending second-moment closure used in the present study predicts the flow in the impinging stagnation region very well [8].

7. Conclusions

An evaluation of the turbulence models is performed for a turbulent natural convection in a rectangular cavity together with the two-layer, SST, V2-f , SMC-DH and EBM models. The performances of the turbulence models are investigated through a comparison with the available experimental data. In general the performances of the EBM, V2-f and SMC-DH models for the prediction of the mean velocity components and the turbulent quantities are very similar while the two-layer and SST models predict them poorly. There are a lot of wall-related parameters in the SMC-DH model. When one considers the fact that the wall related parameters, which hinders the implementation of the models in the general purpose commercial codes, are not present in the EBM model and its performance is as good as or better than the SMC-DH model, the use of the EBM is highly recommended.

The treatment of turbulent heat fluxes with the EBM is tested for a turbulent natural convection in a rectangular cavity and in a square cavity with different geometries and Rayleigh numbers. The Reynolds stresses are calculated using the same EBM. In general the performances of the AFM and DFM for a prediction of the mean vertical velocity component and temperature, thereby the wall shear stress and the Nusselt number, were similar, and the vertical turbulent quantities were slightly better predicted by the AFM. Since the DFM needs computation of two more transport equations for the turbulent heat fluxes in the two-dimensional situation, the DFM needs a more computational time. Thus, the AFM is a better choice, especially in the three-dimensional situation. The GGDH only predicts an accurate solution for a shear dominant flow, however, the model predicts very poor solutions or invokes a numerical oscillation when applied to a flow with a strong stratification. The LES predicts the mean vertical velocity component and temperature, thereby the Nusselt number, better than the AFM and DFM. However, it predicts a poor solution for the turbulent quantities.

A two-dimensional numerical simulation is performed for a natural convection between bottom-hot and top-cold walls by using the elliptic-blending second-moment closure for a Rayleigh number ranging from $Ra = 2\times10^6$ to $Ra = 10^9$ and the computed results are compared with the experimental correlations, T-RANS and LES results. The roll structure, local and cell-averaged Nusselt numbers, long-term mean tempera-

ture and its variance are examined. The predicted cell-averaged Nusselt numbers follow different the correlations in the 'soft' and 'hard' convective turbulence regions and the maximum difference between the present computation and previous correlations was within 5%. These results show that the elliptic-blending second-moment closure with an algebraic flux model predicts very accurately the Rayleigh-Benard convection and its use in a simulation for a higher Rayleigh number region is highly recommended.

Acknowledgement

This study has been supported by the Nuclear Research and Development Program of the Ministry of Education Science and Technology of Korea.

References

[1] K. Hanjalic, One-point closure models for buoyancy-driven turbulent flows, *Annu. Rev. Fluid Mech*., 34 (2002) 321-347.

[2] T. J. Heindel, S. Ramadhyani and F. P. Incropera, Assessment of turbulence models for natural convection in an enclosure, *Numer. Heat Transfer, Part B* 26 (1994) 147-172.

[3] B. E. Launder and B. I. Sharma, Application of the energy dissipation model of turbulence to the calculation of near spinning disc, *Lett. in Heat and Mass Transfer*, 1 (1974) 131-138.

[4] H. C. Chen and V. C. Patel, Near-wall turbulence models for complex flows including separation, *AIAA J*., 26 (1988) 641-648.

[5] G. Medic and P. A. Durbin, Toward Improved prediction of heat transfer on turbine blades, *J. Turbomachinery*, 124 (2002) 187-192.

[6] S. K. Choi, E. K. Kim and S. O. Kim, Computation of turbulent natural convection in a rectangular cavity with the $k-\varepsilon-v^2-f$ model, Numer. *Heat Transfer, Part B*, 45 (2004) 159-179.

[7] F. R. Menter, Two-equation eddy-viscosity turbulence model for engineering applications, *AIAA J*., 32 (1994) 1598-1605.

[8] L. Thielen, K. Hanjalic, H. Jonker and R. Manceau, Prediction of flow and heat transfer in multiple Impinging jets with an elliptic-blending second-moment closure, *Int. J. Heat Mass Transfer*, 48 (2005) 1583-1598.

[9] S. K. Choi and S. O. Kim, Computation of a turbulent natural convection in a rectangular cavity with the elliptic-blending second-moment closure, *Int. Comm. Heat Mass Transfer*, 33 (2006) 1217-1224.

[10] K. V. King, *Turbulent natural convection in rectangular air cavities*, Ph.D Thesis, Queen Mary College, University of London, UK, (1989).

[11] N. Z. Ince and B. E. Launder, On the computation of buoyancy-driven turbulent flows in rectangular enclosures, *Int. J. Heat Fluid Flow,* 10 (1989) 110-117.

[12] S. Kenjeres and K. Hanjalic, Prediction of turbulent thermal convection in concentric and eccentric annuli, *Int. J. Heat Fluid Flow*, 16 (1995) 428-439.

[13] T. W. J. Peeters and R. A. W. M. Henkes, The Reynolds-stress model of turbulence applied to the natural-convection boundary layer along a heated vertical plate, *Int. J. Heat Mass Transfer*, 35 (1992) 403-420.

[14] H. S. Dol and K. Hanjalic, Computational study of turbulent natural convection in a side-heated near-cubic enclosure at a high Rayleigh number, *Int. J. Heat Mass Transfer*, 44 (2001) 2323-2344.

[15] S. K. Choi, E. K. Kim, M. H. Wi and S. O. Kim, Computation of a turbulent natural convection in a rectangular cavity with the low-Reynolds-number differential stress and flux model, *KSME Int. J*. 18 (2004) 1782-1798.

[16] J. K. Shin, J. S. An and Y. D. Choi, Elliptic relaxation second moment closure for turbulent heat flux, Proceed. 4th Int. Symp. Turbulence and Shear Flow Phenomenon, Williasburg, U. S. A., (2005) 271-277.

[17] S. V. Patankar, *Numerical heat transfer and fluid flow*, Hemisphere, New York, USA, (1988).

[18] J. Zhu, A low-diffusive and oscillation free convection scheme, *Comm. Appl. Numer. Methods*, 7 (1991) 225-232.

[19] R. Cheesewright, K. J. King and S. Ziai, Experimental data for the validation of computer codes for the prediction of two-dimensional buoyant cavity flows, Proceedings of ASME Meeting, HTD 60 (1986) 75-86.

[20] Y. S. Tian and T. G. Karayiannis, Low turbulence natural convection in an air filled square cavity part I: the thermal and fluid flow fields, *Int. J. Heat Mass Transfer*, 43 (2000) 849-866.

[21] S. H. Peng and L. Davidson, Large eddy simulation of turbulent buoyant flow in a confined cavity, *Int. J. Heat Fluid Flow*, 22 (2001) 323-331.

[22] S. Kenjeres, Numerical modeling of complex buoyancy-driven flows. Ph.D Thesis, Delft University of Technology, The Netherlands (1998).

[23] S. Kenjeres and K. Hanjalic, Convective rolls and heat transfer in finite-length Rayleigh-Benard convection: A two-dimensional numerical study, Phys. Rev. E, 62 (2000) 7987-7998.

[24] S. Kenjeres and K. Hanjalic, Transient analysis of Rayleigh-Benard convection with a RANS model, *Int. J. Heat Fluid Flow*, 20 (1999) 329-340.

[25] S. Kenjeres and K. Hanjalic, LES, T-RANS and hybrid simulations of thermal convection at high Ra numbers, *Int. J. Heat Fluid Flow*, 27 (2006) 800-810.

[26] S. Kenjeres and K. Hanjalic, LES, Numerical insight into flow structure in ultraturbulent thermal convection, *Phys. Rev. E*, 66 (2002) 036307 1-5.

[27] X. Z. Wu, A. Libchaber, Scaling relation in thermal turbulence, Phys. Rev. A. 40 (1992) 842-845.

[28] S. H. Peng, K. Hanjalic and L. Davidson, Large-eddy simulation and deduced scaling analysis of Rayleigh-Benard convection up to $Ra=10^9$, *J. Turbulence* 7 (2006) 1-29.

[29] J. J. Niemela, L. Skrbek, K. R., Sreenivasan and R. J. Donnelly, Turbulent convection at very high Rayleigh numbers, *Nature* 404 (2000) 837-840.

Seok-Ki Choi is a principal researcher at the Korea Atomic Energy Research Institute since 1990. He received BS and MS degrees from the Seoul National University, Korea and Ph.D degree from the University of Iowa, U.S.A. His research interests are CFD, turbulence modeling and thermal-hydraulic analysis and design of nuclear fast reactor. He is author and co-author of more than 130 publications including journal and conference papers. He is members of KSME, ASME, KNS and is an associate editor of KSCFE.

Seong-O Kim is a principal researcher at the Korea Atomic Energy Research Institute. He received his BS degree from the Jeonnam National University and MS degree from KAIST, Korea. He is an expert on the thermal-hydraulic design of both light water reactor and liquid metal reactor. He has served as a project manager of thermal-hydraulic design of nuclear fast reactor since 2003. He published many papers on thermal hydraulics of nuclear reactors and many patents. He is members of KNS and KSCFE.